Magnetic Stars, 2011, pp. 199 – 214

Some Precautions to Measurements of Weak Magnetic Fields Based on Statistical Processing of Zeeman Features

Bochkarev N. G.[1], **Karitskaya E. A.**[2]

[1] Sternberg Astronomical Institute, Moscow, Russia
[2] Institute of Astronomy RAS, Moscow, Russia

Abstract. Some precautions to the measurements of weak stellar magnetic fields by the least squares technique are considered on the example of Cyg X–1 = HDE 226868 (the optical counterpart is an O9.7 supergiant). The V/I circular polarization spectra obtained during our spectropolarimetric FORS1 VLT observations have variable sloped continuum components not belonging to the object. It is shown that such components should be removed, otherwise these spurious sloped continua yield biased results. For HDE 226868 the magnetic field bias $\Delta \langle B_z \rangle$ varies from 20 G to 100 G, which is comparable to its value. The slopes of the I–spectra have a smaller influence on $\langle B_z \rangle$ result but they should be subtracted too. Initial I and V/I–spectra cleaning, the effects from the deviating points and their influence on the results of $\langle B_z \rangle$ measurements are also considered.

Key words: spectropolarimetry – Stokes parameter V for circular polarization – circular polarization spectra: Zeeman spectral line features – spectropolarimetric data cleaning – stellar magnetic fields: longitudinal component – magnetic field measurement: least squares technique: affecting factors – magnetic field spurious component – stars: O–supergiant – stars: X–ray binaries: Cygnus X–1

1 Introduction

Investigations of stellar magnetic fields are quickly progressing. More and more faint and distant stars, as well as the stars with weak magnetic fields become the targets for observations. As a result, the method of measuring the longitudinal component of magnetic fields averaged over the picture plane $\langle B_z \rangle$ based on the Zeeman feature statistical processing by the least squares technique for the analysis of spectropolarimetric observations brought forward by Landstreet (1982) is more and more widely used. The O–star 100 – 300 G strong magnetic fields were measured over the past few years.

The main goal of this paper is to draw attention to different factors affecting weak magnetic field measurements based on the Zeeman feature statistical processing of the circular polarization spectrum $V(\lambda)$ along with the full intensity one $I(\lambda)$. Here λ is the wavelength; V and I are the Stokes parameters describing circular polarization, and full intensity spectra, respectively.

To present quantitative results, we take an example of the VLT FORS1 spectropolarimetric observations of a O9.7 supergiant HDE 226868 (the optical component of the famous X–ray binary Cyg X–1) with a rather weak variable magnetic field $\langle B_z \rangle \lesssim 130$ G (Karitskaya et al., 2009, 2010; see

also Karitskaya et al., 2011 in this volume).

The statistical method has been already applied (and carefully tested) in previous studies of bright magnetic stars (e. g. Hubrig et al., 2004; Bagnulo et al., 2002, 2006) which usually do not have significant interstellar or intrinsic linear polarization, but a rather strong $\langle B_z\rangle = 500-2000$ G. In contrast, Cyg X–1 has a weaker $\langle B_z\rangle$ and a strong interstellar/circumstellar linear polarization. For this reason we had to meet some precautions in the magnetic field measurements of this system and adapt the method for similar conditions.

In this paper we consider four effects distorting the $\langle B_z\rangle$ estimates. The first one involves the features in the I and V/I spectra, formed outside the stellar photosphere (Section 4.3). We concentrate on the distorting influence of the wavelength dependence (slopes) of the continuum $C_{V/I}(\lambda)$ in the spectra of the degree of circular polarization $p_V = V/I$ (Section 5). If we ignore $C_{V/I}(\lambda)$ wavelength dependence, even a spurious magnetic field may be produced (Subsection 5.3.2). The V/I continuum plays the role of the background for the spectral–line Zeeman features carrying the information about the magnetic field. Therefore, the sloped V/I continuum $C_{V/I}(\lambda)$ biases measured $\langle B_z\rangle$ by a value comparable to or exceeding the measurement accuracy, and therefore should be taken into account. A couple of other distorting effects in the $\langle B_z\rangle$ measurements by the statistical method are briefly considered in two short Sections 6 and 7 of this paper: the influence of non-removed slopes of the continua of the spectra of intensity I and effects from the presence of a number (though small) of wavelengths λ_i with large ($>3.5\,\sigma$) residual deviations in the V/I spectra. Both effects take place in the $\langle B_z\rangle$ measurements independently of the $C_{V/I}(\lambda)$ presence and shape.

2 Some Abbreviations and Designations

Hereinafter we denote the V–profiles of spectral lines caused by the Zeeman effect as Zeeman waves.

Abbreviation LST means the Least Squares Technique for the determination of the mean longitudinal magnetic field $\langle B_z\rangle$ based on the ordinary least squares method.

Hereinafter we use the symbol C for the continual (more exactly, quasi–continual) component of the spectral distribution of the value specified as the subscript; e. g., $C_I(\lambda)$, $C_V(\lambda)$ and $C_{V/I}(\lambda)$ mean, respectively, the continual components of the wavelength distributions of the Stokes parameters $I(\lambda)$, $V(\lambda)$ and their ratio V/I, which is the spectrum of the degree of circular polarization p_V.

In what follows, S means the slope of the corresponding continuum: e. g., S_V means the slope of $C_V(\lambda)$. The words "slope" and "trend" are hereinafter used as synonyms designating the derivation of the continuum as a rule averaged over the observed spectral range, e. g., $S_{V/I} = \langle \mathrm{d}C_{V/I}/\mathrm{d}\lambda\rangle$ or some approximation of it.

The symbol σ corresponds to the "standard" (root–mean–square) deviation of the expectation value for the "normal" (Gauss) statistics. If σ has a subscript, the latter refers to the value for which the deviation is given, e. g., σ_I means the standard deviation of the Stokes parameter I.

3 Magnetic Field Measurement Using the Least Squares Technique

The longitudinal component of magnetic fields averaged over the picture plane $\langle B_z\rangle$ is often determined by processing the spectra of circular polarization $V(\lambda)$ and intensity $I(\lambda)$. The equation valid for weak fields (typically $\langle B_z\rangle \lesssim 1-10$ kG) when the Zeeman splitting is small as compared to the intrinsic line broadening (e. g., Landstreet, 1982) is

$$\frac{V}{I} = -C_Z\, g_{\rm eff}\, \lambda^2\, \frac{1}{I}\, \frac{\mathrm{d}I}{\mathrm{d}\lambda}\, \langle B_z\rangle + \frac{V_0}{I_0} = -C_Z\, g_{\rm eff}\, \lambda\, \frac{\mathrm{d}\log I}{\mathrm{d}\log\lambda}\, \langle B_z\rangle + b, \qquad (1)$$

where $g_{\rm eff}$ is the effective Landé factor, $b = V_0/I_0 = const$ is a quantity not depending on λ,

$$C_Z \cong \frac{e}{4\pi m_e c^2} = 4.67 \cdot 10^{-13}\ \text{Å}^{-1}\text{G}^{-1}. \tag{2}$$

Here m_e is the electron mass; c is the speed of light; $\mathrm{d}I/\mathrm{d}\lambda$ is the derivative of the Stokes I parameter. Logarithmic derivative

$$\gamma(\lambda) = \frac{\mathrm{d}\log I}{\mathrm{d}\log \lambda} \tag{3}$$

in Eq. (1) is a dimensionless quantity showing the approximation of $I(\lambda)$ by a power–law function $I \sim \lambda^{\gamma}$, i. e., the function $I(\lambda)$ slope in the log–log scale.

The statistical method for the solution of Eq. (1) based on the ordinary least squares technique is widely used to determine $\langle B_z \rangle$. For a detailed description of the method see, e. g., Bagnulo et al. (2002, 2006) and Hubrig et al. (2004). In this section we are mainly following these papers.

The mean longitudinal magnetic field $\langle B_z \rangle$ is determined from the slope of the linear regression of $(\mathbf{Y} - \mathbf{X})$, where $\mathbf{Y}$ and $\mathbf{X}$ are the sets of N independent measurements ($i = 1, 2, \ldots, N$) of the left part of the Eq. (1) and of the factor at $\langle B_z \rangle$ in its right part:

$$Y_i = X_i \cdot \langle B_z \rangle + b \qquad (i = 1, 2, \ldots, N). \tag{4}$$

Here

$$Y_i = \frac{V_i}{I_i} \tag{5}$$

and

$$X_i = -4.67 \cdot 10^{-13}\, g_{\rm eff}\, \lambda_i^2\, \frac{1}{I_i}\, \frac{\mathrm{d}I_i}{\mathrm{d}\lambda_i}, \tag{6}$$

wavelengths λ_i are in Angströms (Å) and the longitudinal field $\langle B_z \rangle$ is in Gauss (G).

Since the obtained uncertainties σ_X for X_i and σ_Y for Y_i satisfy the inequality $\langle B_z \rangle\, \sigma_X \ll \sigma_Y$ (Bagnulo et al., 2006), in real cases LST can be used for the calculations of the $(\mathbf{Y} - \mathbf{X})$ regression (e. g. Isobe et al., 1990). The mean longitudinal magnetic field $\langle B_z \rangle$ and its uncertainty σ_{B_Z}, as well as the constant b and its uncertainty are determined by applying LST to the system of equations (4) with weights $w_i \propto [\sigma_I(\lambda_i)]^{-2} \propto I(\lambda_i)$. Here the values of $I(\lambda_i)$ are in counts per pixel along dispersion (counts integrated in the pixel column across the dispersion). The derivative $\mathrm{d}I/\mathrm{d}\lambda$ is usually calculated by the simplest two-point numerical approximation.

The method is a statistical one: it permits to measure $\langle B_z \rangle$ using the Zeeman features for all the observed spectral lines and, as a result, increases sensitivity.

4 Sample Object and Its Spectropolarimetric Observations

4.1 Sample Object Cygnus X–1 = HDE 226868

We consider the spectropolarimetric observations of the optical counterpart of the X–ray binary Cyg X–1 = HDE 226868 as an example. The main parameters of the system are:

- Apparent magnitude $m_V \approx 9^m$;
- The primary (optical) component is an O9.7 Iab supergiant;
- The secondary (X–ray) component is an accreting black hole;
- $> 95\,\%$ of emission in the optical range is produced by the O–star;

- The optical spectrum mostly contains the O–supergiant photospheric absorption lines; the accretion–structure emission components are strong in He II 4686 Å and Hα profiles only; weak P Cyg stellar–wind components appear in H and He I lines as well as in some O II lines (Karitskaya et al., 2008);
- Interstellar/circumstellar reddening $E(B-V)=1.07^m$ and extinction $A_V=3.36^m$;
- Interstellar/circumstellar linear polarization $\sim 5\,\%$;
- Stellar wind $\dot{M}\sim(2-3)\cdot 10^{-6} M_\odot$/yr (Gies et al., 2003);
- Weak chemical peculiarities (mainly He, N, Si excess by a factor of 2.5 – 8: see Karitskaya, 2007; Karitskaya et al., 2008);
- moderate rotation velocity $V\sin i\approx 115$ km/s (Karitskaya et al., 2008);
- magnetic field ~ 100 G has been discovered (Karitskaya et al., 2009, 2010, 2011).

4.2 Spectropolarimetric Observations of Cyg X–1 = HDE 226868

The sampled object HDE 226868 = Cyg X–1 has been observed with the Focal Reducer/Low Dispersion Spectrograph (FORS1) of the 8.2 m Very Large Telescope (VLT) (Mount Paranal, Chile). The observations were conducted in the framework of our programs 079.D–0549 and 381.D–0138 (Karitskaya et al., 2009, 2010, 2011). We used the FORS1 spectropolarimetry (PMOS) mode with single target (fast) acquisition mode. We selected grism 1200 B without filters and slit $0\farcs4$, which permitted us to cover the spectral range of 3680 – 5129 Å with the spectral resolution of $R\approx 4000$. The spectra of two Stokes parameters were measured: intensity I and circular polarization V (more exactly V/I).

The formally calculated signal–to–noise ratio S/N for the I spectra (calculated as the square root of the total number of counts per pixel, see the end of Section 3) varied along the spectrum and from spectrum to spectrum within the range $S/N=1500-3500$.

The 1.3–hour long observations per night in the service mode were conducted during 13 nights. We obtained six spectra over the nights of June 18/19 – July 9/10, 2007 and seven spectra over the nights of July 14/15 – July 30/31, 2008. The date (night) of each observation is given in column 2 of Table 1.

Each observation consisted of eight 500–second exposures. The Wollaston prism inserted into the optical path permits us to record simultaneously the spectra of the ordinary and extraordinary beams. Thus, one observation contains 16 spectra in total.

The position angle α of the quarter–wave plate was changed from $+45^\circ$ to -45° or vice versa every second exposure, i. e., we were performing the sequence α: $+45^\circ$, -45°, -45°, $+45^\circ$, $+45^\circ$, -45°, -45°, and $+45^\circ$. The FORS1/2 user manual explains that the instrumental polarization cancels out to the first order if the Stokes V is obtained from a pair of expositions

$$\frac{V}{I}=\frac{1}{2}\left\{\left(\frac{f^o-f^e}{f^o+f^e}\right)_{\alpha=-45^\circ}-\left(\frac{f^o-f^e}{f^o+f^e}\right)_{\alpha=+45^\circ}\right\}, \qquad (7)$$

where f^o and f^e are the ordinary and extraordinary beams, respectively, and α is the position angle of the retarder wave plate. Here all the values except for α are measured in counts per pixel integrated across the dispersion.

We thus obtained a total of 13 pairs of spectra (intensity I – circular polarization V/I), each pair being based on eight exposures (16 spectra: 8 f^o and 8 f^e) per each night (Karitskaya et al., 2009, 2010, 2011). S. Hubrig performed a preliminary processing of CCD images. The analysis of

the 2007 data has been fulfilled by S. Hubrig and M. Schöller and independently by N. G. B. We adopt the effective Landé factor $g_{\rm eff} = 1.07$ according to Hubrig et al. (2008). We used the results of the primary processing for the calculation of $\langle B_z \rangle$, taking into account the effects of various factors described in this paper.

4.3 The Effect of Initial Cleaning of I and V/I Spectra on the Results of $\langle \mathbf{B_z} \rangle$ Measurement

Before starting the $\langle B_z \rangle$ calculations, we carefully eliminated from the I and V/I–spectra all the features that could distort the results. Namely, we inspected all the I–spectra and excluded from the further analysis all the fragments of both I and V/I–spectra containing the features formed outside the photosphere of the Cyg X–1 optical component:

1) interstellar lines and narrow diffuse interstellar bands (DIBs);

2) defects (including residual cosmic ray traces that remained after the standard observation processing);

3) He II 4686 Å line with a complicated profile including the accretion–structure emission component (the second emission line Hα is situated outside the spectral range of our VLT observations);

4) emission components of the lines with the P Cyg effect.

5) In addition we removed some λ intervals containing no observed lines besides noise.

We found no pollution by telluric lines in our spectra.

After these procedures we made several tests briefly described by Karitskaya et al. (2009, 2010, 2011).

Table 1 illustrates the effect of cleaning on the results of LST application to the $\langle B_z \rangle$ measurement. The values for the 13 observations described in Section 4.2 are listed. Column 3, B_1, shows the results of applying the LST to determine $\langle B_z \rangle$ on the basis of full I and V/I spectra, i. e., all the ~ 4000 observed spectral points (pixels) over the range of 3680 – 5129 Å. The 5th column (B_2) contains the $\langle B_z \rangle$ estimates made by the same method (LST) but on the basis of the cleaned spectra (after omitting the wavelength intervals listed in items 1 – 5).

Column 4, ΔB_1 contains the difference between the magnetic field values $\langle B_z \rangle$ obtained from cleaned and uncleaned spectra. All the corrections are positive with one exception. It is a natural result of the exclusion of "noisy" spectral features which have no relation to the Zeeman waves produced by the photospheric magnetic field.

The exception is the 1st observation that actually shows a zero magnetic field $|B_i| \ll \sigma$ for all i, and about a zero correction $|\Delta B_1| < \sigma$. It is possible that during the first night a manifestation of an active process in the X–ray binary system was registered. Namely, the depth of all the observed Balmer hydrogen lines was significantly smaller in the 1st night than during any other observational sets. It is probably a result of an overlap of the accreting gas emission lines with the O–star photospheric lines.

In our sampled observations the typical value of the correction ΔB_1 varies within the range of $30 \div 60$ G. The maximal bias is slightly above 100 G. Hence, these corrected values are comparable with or exceed the measurement accuracy and, therefore, should be taken into account.

In our case the largest contribution to ΔB_1 comes from very sharp and strong interstellar H and K Ca II lines (3968 Å and 3934 Å). Inside the line profiles the absolute values of the dimensionless slope of the I–spectra γ (see Eq. (3)) reach the value several times higher than $|\gamma|$ for any other

Table 1: Corrections to the mean longitudinal magnetic field strengths $\langle B_z \rangle$ determined by the least squares technique from the VLT FORS1 spectropolarimetric observations of HDE 226868 = Cyg X–1

No.	Night	B_1^*	ΔB_1^*	B_2^*	ΔB_2^*	B_3^*	ΔB_3^*	B_4^*
(1)	(2)	(3)	(4)	(5)	(6)	(7)	(8)	(9)
1	18–19/06/07	$+8 \pm 40$	-3	$+5 \pm 44$	-33	-28 ± 31	$+22$	-6 ± 28
2	19–20/06/07	$+40 \pm 31$	$+21$	$+61 \pm 39$	-23	$+38 \pm 26$	$+1$	$+37 \pm 22$
3	20–21/06/07	$+100 \pm 29$	$+7$	$+107 \pm 37$	-61	$+46 \pm 25$	$+12$	$+58 \pm 21$
4	25–26/06/07	-30 ± 38	$+38$	$+8 \pm 45$	-36	-28 ± 31	$+50$	$+22 \pm 28$
5	29–30/06/07	$+101 \pm 27$	$+27$	$+128 \pm 37$	-69	$+59 \pm 22$	-11	$+48 \pm 20$
6	09–10/07/07	$+166 \pm 25$	$+47$	$+213 \pm 36$	-74	$+139 \pm 20$	-38	$+101 \pm 18$
7	14–15/07/08	$+62 \pm 26$	$+56$	$+121 \pm 34$	-73	$+48 \pm 28$	$+1$	$+49 \pm 23$
8	15–16/07/08	$+33 \pm 25$	$+40$	$+71 \pm 31$	-45	$+9 \pm 26$	$+13$	$+22 \pm 22$
9	16–17/07/08	$+123 \pm 26$	$+27$	$+154 \pm 33$	-66	$+88 \pm 28$	-8	$+80 \pm 23$
10	17–18/07/08	$+43 \pm 22$	$+36$	$+80 \pm 35$	-51	$+29 \pm 22$	-5	$+24 \pm 19$
11	23–24/07/08	$+13 \pm 22$	$+61$	$+80 \pm 35$	-99	-19 ± 24	$+3$	-16 ± 20
12	24–25/07/08	$+47 \pm 22$	$+52$	$+101 \pm 29$	-72	$+29 \pm 23$	-2	$+27 \pm 19$
13	30–31/07/08	$+121 \pm 20$	$+110$	$+231 \pm 31$	-70	$+161 \pm 25$	-33	$+128 \pm 21$

* Notes:
B_1 are $\langle B_z \rangle$ calculated by applying LST to all spectral points (pixels) of the I and V/I–spectra.
B_2 are $\langle B_z \rangle$ calculated from the cleaned spectra (all the spectral features mentioned in Section 4.3 are omitted).
B_3, after the V/I trends were removed (see Section 5.4) from the spectra used for the calculations B_2.
B_4, after corrections for the pseudo–continua of the I–spectra (see Section 6) and deletion of the spectral points with large residual deviations (see Section 7).
Values in the last column correspond to the final results of the $\langle B_z \rangle$ determination, given in (Karitskaya et al., 2009, 2010, 2011).
For all the B_i the standard deviations $\pm\sigma$ are given.
$\Delta B_i = B_{i+1} - B_i$, $i = 1, 2, 3$ are the corrected values.
All magnetic field values are expressed in Gauss.

spectral line becoming comparable with its upper limit approximately equal to the spectral resolution R of the equipment used ($\gamma \approx R$). The position instability of the FORS1, reaching 0.9 pixel (see FORS1/2 manual) can probably create a small shift along the dispersion of the V/I spectrum with respect to the I one resulting in a significant bias of the measured $\langle B_z \rangle$ values.

Other noise–creating spectral features listed in this section bring a smaller, however comparable contribution to ΔB_1. For instance, in one of the 13 observations we found a 1 pixel–wide defect (probably, a cosmic ray trace that has not been removed); its elimination changes the $\langle B_z \rangle$ estimate by about 100 G.

5 V/I–trends

5.1 The Causes of Origin of Wavelength–Dependent Circularly Polarized Optical Continuum

Let us consider several obvious causes of the origin of wavelength–dependent circularly polarized continuum in star observations.

Polars are the most famous sources of wavelength–dependent, strongly (up to $\sim 30\,\%$) variable, linearly and circularly polarized continual radiation in the optical range, produced by the emis-

sion of strongly magnetized plasma changing its orientation with the object rotation phases. Some other types of variable stars have a weak intrinsic wavelength-dependent circularly polarized optical continuum, usually of a similar origin.

In contrast to the previous case, the optical continuum from distant stars gets a wavelength–dependent linearly and circularly polarized component on its way from the star to the telescope due to interstellar/circumstellar linear (up to $\approx 10\,\%$) and weak circular ($< 0.05\,\%$) polarization. The polarization is produced by extinction due to non-spherical interstellar dust grains, partially aligned with respect to the interstellar magnetic field.

Such an origin of optical polarization is typical for luminous stars: first of all for supergiants and hot main-sequence early B and O–type stars. Interstellar polarization has a specific wavelength dependence usually described by the Serkowski formula for linear polarization, and for the circular one characterized by the Stokes V parameter sign change within the optical range.

In addition to the above–mentioned causes, the measured polarized continuum can arise inside the telescope and its recording equipment. Indeed, any spectropolarimeter has a cross–talk (conversion) between linear and circular polarization modes, thus creating a spurious circularly polarized wavelength–dependent continual component of radiation for the stars with an intrinsic or/and interstellar linear polarization.

As a result of, mainly, the last two cases, the spectra of objects selected for magnetic field measurements are more and more often polluted with the Stokes V parameter and the V/I ratio showing the wavelength–dependent continuum components.

5.2 Observed V/I Spectra Slopes (V/I–trends) and Their Probable Origin

For our sample object HDE 226868 = Cyg X–1 the continua $C_{V/I}(\lambda)$ of all the V/I spectra show slight slopes (V/I–trends). Within the spectral range $\lambda\lambda 3680 - 5129$ Å the V/I continua appear to be almost linear, increasing with λ (Fig. 1 and Fig. 2) by

$$\Delta C_{V/I} = C_{V/I}(5129\,\text{Å}) - C_{V/I}(3680\,\text{Å}) = 0.053\,\% - 0.17\,\%. \tag{8}$$

The slope value

$$S = \mathrm{d}C_{V/I}/\mathrm{d}\lambda \approx \Delta C_{V/I}/\Delta\lambda = (0.37 - 1.2)\cdot 10^{-6}\ \text{Å}^{-1} \tag{9}$$

varies irregularly from night to night (Fig. 2). The values of the slopes S are determined on the significance level $(20 - 50)\,\sigma_S$.

The V/I spectrum slopes cannot be explained by Cyg X–1 interstellar or/and intrinsic circular polarization (both are present but have smaller values: $\approx 0.02 - 0.03\%$ each, Michalsky & Swedlung, 1977). The most probable reason of the V/I spectrum slopes is a cross–talk between the linear and circular polarizations within the FORS1 analyzing equipment.

If the cross–talk from linear polarization produces a significant part of the circular polarization continuum, we should be careful about the Zeeman wave contamination by the spectral–line features in the linear polarization spectrum. The cross–talk from the features overlapping with the Zeeman waves can produce a distorted $\langle B_z \rangle$ value. Therefore, in the general case for the $\langle B_z \rangle$ measurement in linearly polarized objects, the spectra in all four Stokes parameters should be observed. It is not necessary for stars that only have interstellar polarization and have no intrinsic linear polarization since the interstellar polarization is produced by the interstellar dust grains that have a continual extinction in the optical range without any narrow spectral features.

The observed Cyg X–1 radiation possesses both interstellar and intrinsic components of linear polarization. However, the intrinsic one, which manifested itself as a component varying with the orbital phase of the binary star contains but a small part ($\approx 1/50$) of total polarization. Nagae et al. (2009) state that the 60 Å spectral resolution allows them to see the Hα emission line, but there

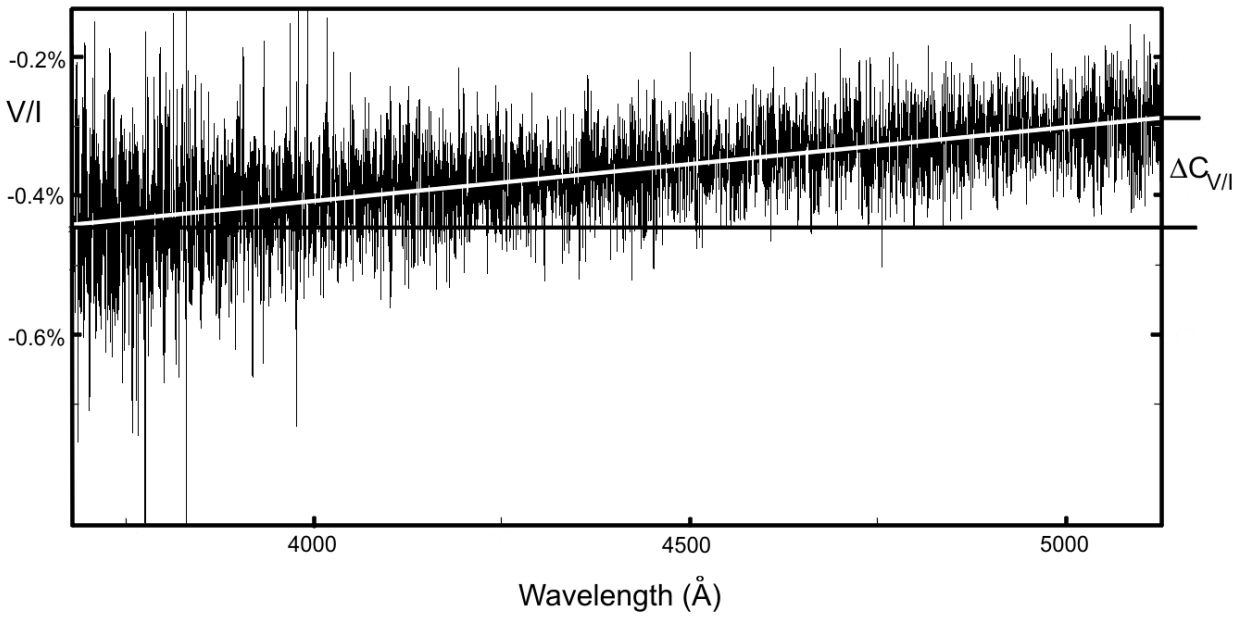

Figure 1: The V/I–spectrum of Cyg X–1 for the night 14/15 July 2008 (noisy line) and its linear regression (thick straight white sloped line). The continuum difference $\Delta C_{V/I}$ (see Eq. (8)) is marked.

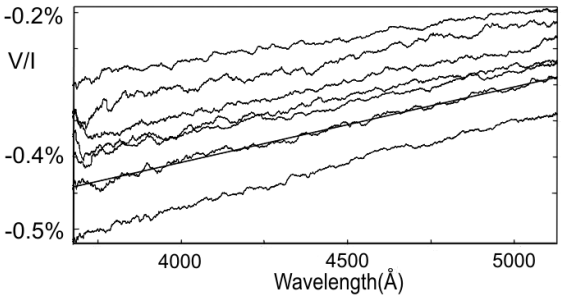

Figure 2: All the 2008 V/I spectra smoothed with a 50 Å–wide Gaussian filter (broken lines) and the linear regression (straight line) for the spectrum shown in Fig. 1. It is visible that the linear approximation is surprisingly suitable for the V/I trend description.

is no demonstration of it in the linear polarization at the accuracy level of 0.02 %. This line is 12 Å–wide. It means that the linear polarization continuum distortion is less than 0.1 %. The lines have a larger optical depth in respect to the continuum and therefore may be partially depolarized with respect to it. Since Hα is the strongest emission line, it may be expected to undergo the maximal depolarization.

According to the FORS1/2 user manual, the zero angle chromatism of the retarding plate stays within $\pm 1/20$ rad. Consequently, the circular polarization of the spectral–line profiles due to the cross–talk from linear polarization most likely does not exceed $0.005 - 0.01\%$, which is several times lower than the values obtained by Karitskaya et al. (2011). Thus, the distortion of the magnetic field values by the effect discussed above may be expected to be several times smaller than the measured value.

5.3 Influence of V/I trends on the Results of $\langle B_z \rangle$ Measurements

Application of the least squares technique to the data with non–removed V/I trends results in the distortion of the obtained $\langle B_z \rangle$ value and its significance level. There are at least two causes for it:

1) Strong violation of the residual Gaussian statistics;

2) Appearance of a spurious $\langle B_z \rangle$ component produced by a sloped V/I continuum without any Zeeman wave in the I spectra.

Let us consider briefly each one of them.

5.3.1 Violation of the Residual Gaussian Statistics

a) The absence of the V/I trend ($C_{V/I}(\lambda) = const$ and, consequently, $S = 0$, see Eqs. (8) and (9)), means that:

- The least squares method is valid, i. e., LST yields a correct value for $\langle B_z \rangle$.
- Distribution F of residuals ε_i of the system (4) solution is described by the Gaussian function

$$F(x_i) = \frac{1}{\sqrt{2\pi}} e^{-x_i^2/2}, \tag{10}$$

  where $x_i = \varepsilon_i / \sigma_\varepsilon$.

- The "normal" statistical significance $P(x/\sigma_x)$ of a result x measured to "accuracy" σ_x in accordance with the Laplace function, and the probability of obtaining a false result $(1-P)$ depends on x/σ_x

$$1 - P(x/\sigma_x) = \sqrt{\frac{\pi}{2}} \int\limits_{|x|/\sigma_x}^{\infty} e^{-u^2/2} du. \tag{11}$$

b) If V/I trend exists:

- The least squares method is still valid, which means that LST yields a mathematically correct solution for $\langle B_z \rangle$.

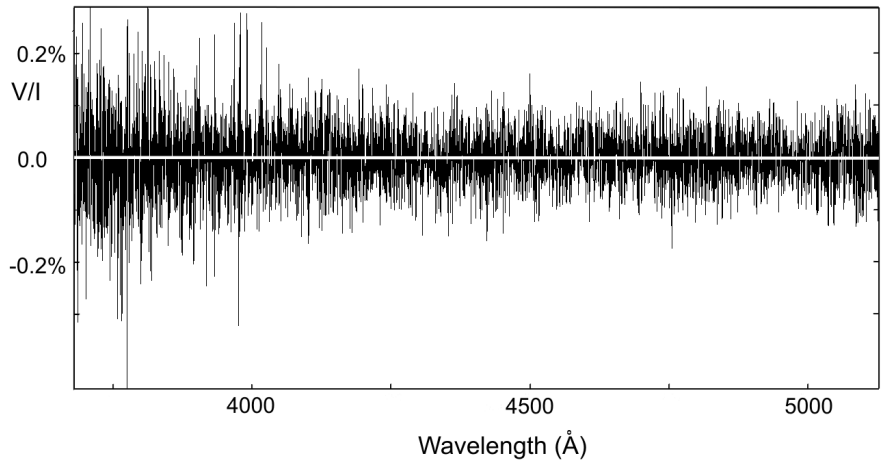

Figure 3: The same Cyg X–1 V/I spectrum as in Fig. 1, but the trend of its continuum $C_{V/I}(\lambda)$ shown in Fig. 1 by the thick straight white line has now been removed.

- If the trend is present, the distribution of residuals broadens beyond the Gaussian function. For instance, the scatter along the vertical axis of the measured $(V/I)_i$ points in the V/I spectrum before V/I trend removal (Fig. 1) is broader than after the trend removal (Fig. 3). The trend removal makes the distribution more similar to a Gaussian one (Eq. 10) than before the removal. Although Figures 1 and 3 do not only contain residuals, but also the full measured signal (i. e., residuals plus Zeeman features) then the figures for the residuals would look very similar, because the useful signal in our sample does not exceed a half of $\sigma_{V/I}$. If the trend is strong, i. e., $\Delta C_{V/I} \gg \sigma_{V/I}$, the distribution acquires a broad flat top and steep edges and in the limit $\sigma_{V/I} \to 0$ the shape of the distribution becomes Π–like.
- The relationship between the resulting significance P of the measured value of X and the standard deviations σ_X no longer follows the Laplace function (11), and therefore $(1-P)$ becomes the more underestimated the more is the X/σ_X ratio, and for the large $X/\sigma_X \gtrsim 2-3$ it can be underestimated by orders of magnitude.

5.3.2 Appearance of a Spurious $\langle B_z \rangle$ Component

Let us consider the simplest example of a purely linear dependence of V/I on wavelength λ with no statistic fluctuations ($\sigma_{V/I} \to 0$) and without a Zeeman wave (actual $\langle B_z \rangle = 0$).

It means that within the wavelength interval $\lambda_1 \leq \lambda \leq \lambda_2$

$$V(\lambda)/I(\lambda) = C_{V/I}(\lambda) = S \cdot \lambda + T. \tag{12}$$

Here $S = \mathrm{d}C_{V/I}(\lambda)/\mathrm{d}\lambda = const$ is value of V/I slope and T is a *const*. For simplicity we adopt $T = 0$.

We suggest also high spectral resolution (step of λ: $\delta\lambda = \lambda_{i+1} - \lambda_i \to 0$) and presence of only one feature (an absorption line) in the intensity spectrum $I(\lambda)$:

$$I(\lambda) = 1 - r_0\, e^{-\left(\frac{\lambda-\lambda_0}{\Delta\lambda_\mathrm{D}}\right)^2}, \tag{13}$$

where $\delta\lambda < \Delta\lambda_\mathrm{D} \ll \lambda_2 - \lambda_1$, $\lambda_0 - \lambda_1 \gg \Delta\lambda_\mathrm{D}$, $\lambda_2 - \lambda_0 \gg \Delta\lambda_\mathrm{D}$ and line depth r_0 is moderate: $\sigma_I \ll r_0 \ll 1$, where σ_I is the intensity measurement accuracy.

Under the described conditions the mean longitudinal magnetic field calculated by LST application to this example is

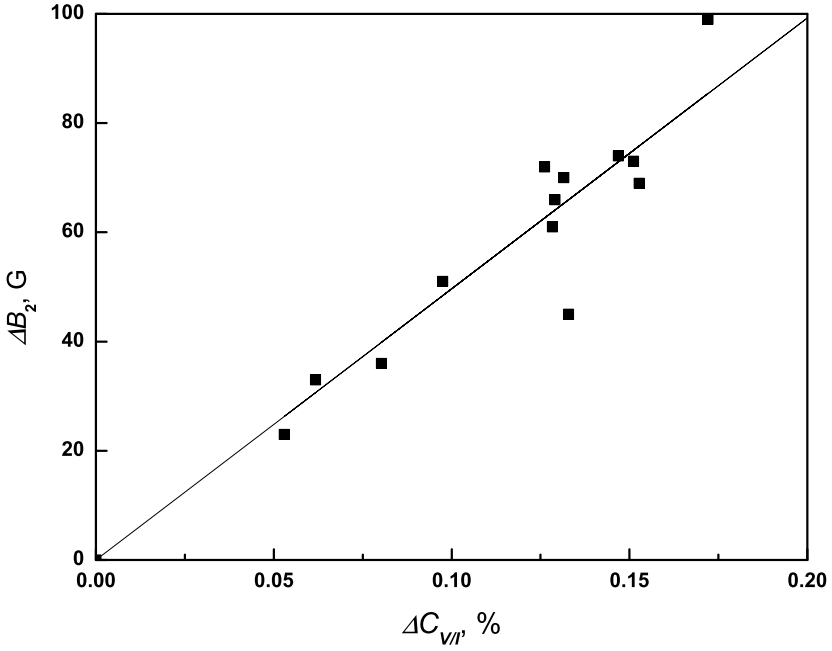

Figure 4: The corrections ΔB_2 versus the slopes $\Delta C_{V/I}$ of V/I continua. The correlation coefficient is equal $r \approx 0.98$.

$$\langle B_z \rangle = 2^{1/2} \, (\Delta\lambda_{\rm D}/\lambda)^2 \, S/(g_{\rm eff} \, C_Z \, r_0), \tag{14}$$

where $g_{\rm eff}$ and C_Z are the constants in Eq. (1).

Thus, in the presented example the LST calculation produces a spurious $\langle B_z \rangle \neq 0$ instead of the actual zero–field. The spurious $\langle B_z \rangle$ is proportional to

$$\langle B_z \rangle_{\rm Spurious} \propto (\Delta\lambda_{\rm D}/\lambda)^2 \, {\rm d}C_{V/I}/{\rm d}\lambda. \tag{15}$$

5.4 Biases of the Measured $\langle \mathbf{B_z} \rangle$ Produced by the V/I–continuum Slope in HDE 226868 = Cyg X–1

The spurious $\langle B_z \rangle$ which follows from the ideal example considered above is given by Eqs. (14) for the slopes obtained from our Cyg X–1 FORS1 observations (see Eq. (8)) is equal to several Gauss only. In reality, there are many lines in the I spectrum and the real spurious component in measured $\langle B_z \rangle$ is several tens of Gauss.

To avoid any influence of the V/I–continuum slope on our $\langle B_z \rangle$ measurements, we subtracted the linear trends from the V/I spectra.

Details are given in Table 1. Columns 5 (B_2) and 7 (B_3) contain the LST estimates of $\langle B_z \rangle$ based on the data before and after removing the V/I trends (slopes), respectively. Column 6 (ΔB_2) shows the differences between these two data sets. One can see that all the corrections have the same sign (in our case all of them are negative). Corrections ΔB_2 and the slopes of the V/I–continua (Eqs. (8) and (9) and Fig. 2) for 13 observations shown in Fig. 4 have a good correlation, $r \approx 0.98$, but not an absolute one $r = 1$, as it follows from Eqs. (14) and (15). In contrast to the simplest example, a

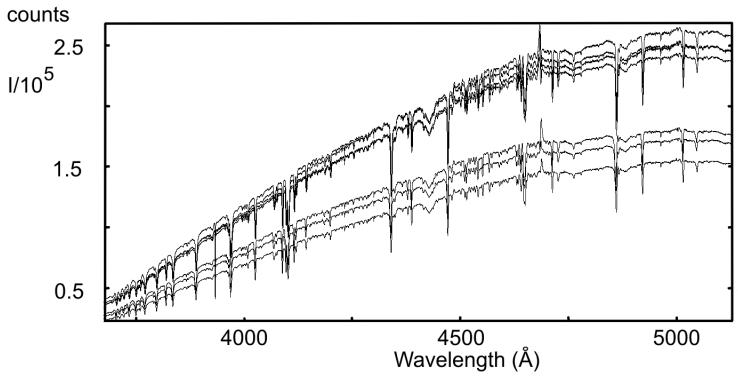

Figure 5: Seven $I(\lambda)$ spectra of Cyg X–1 co-added over each observational night of 2008. The horizontal axis shows the spectral range $\lambda\lambda 3680-5129$ Å; the vertical axis gives intensity I in counts per pixel along dispersion summarized over 16 f^o and f^e spectra consisting each of an I spectrum, see Section 4.2.

real scatter is present with maximal deviations not exceeding $\simeq 15-20$ G. A possible cause for it is noisy observational data. The maximal deviations do not exceed $\sigma_{\langle B_Z\rangle}$.

As it follows from Table 1, after the removal of the slopes, $\langle B_z\rangle$ decreases by $25-100$ G depending on the slope value. Thus, the values of ΔB_2 corrections are comparable to or exceed the measurement accuracy and, therefore, should be taken into account.

It should be mentioned that the calculations of the V/I continuum slope and $\langle B_Z\rangle$ by the LST can be done simultaneously if we apply the least squares method not to the "1D" system of linear equations (4) but to the 2D system (to add the second dimension), replacing it :

$$Y_i = X_i \cdot \langle B_z\rangle + \lambda_i \cdot S + b \qquad (i = 1,\, 2,\, \ldots\, , N). \tag{16}$$

The sought linear regressions $\langle B_Z\rangle$ and S are independent variables. The covariations between them should be zero. The actual calculations support this statement. The correlation coefficients are less than 0.01 and are usually $\sim 10^{-3}$.

6 Influence of the Slopes of I–spectra on $\langle \mathbf{B_z}\rangle$

A set of Cyg X–1 intensity I spectra from 2008 is given in Figure 5. Their continua (pseudo–continua, more exactly) C_I show wavelength–dependent slopes $S_I(\lambda) = \mathrm{d}C_I(\lambda)/\mathrm{d}\lambda$. We normalized the I–spectra to their pseudo–continua.

The wavelength dependence of the I–continuum $C_I(\lambda)$ is produced by:

- the source energy distribution (in our example it is mainly the energy distribution of the O9.7–supergiant emission),
- interstellar reddening (see Section 4.1),
- broad diffuse interstellar bands (DIBs),
- atmospheric extinction,
- the sensitivity of the detector used.

In the case of our observations the absolute values of the dimensionless broadband pseudo-continuum slopes γ from Eq. (3) of the I–spectra (without DIBs influence) reach

$$\gamma = |\mathrm{d}(\log(I(\lambda))/\mathrm{d}(\log(\lambda))| \sim 20.$$

Such maximal values of γ correspond to the shortest λ. In the case of Cyg X–1, the main input in γ is from the strong interstellar reddening of the object.

The removal of the slopes yields the $\langle B_z \rangle$ corrections up to ≤ 3 G. Larger corrections appear as a result of broad–DIBs influence such as $\lambda 4430$ Å and $\lambda 4880$ Å which distort the profile of the Hβ line (Fig. 5). In total, in our case the correction to the I continuum slopes does not exceed 20 G. It is usually smaller than the statistical errors $\sigma_{\langle B_Z \rangle} \geq 20-30$ G.

7 Effects From the Deviating Points

After the above–mentioned reductions the residual deviations from the linear regression (the least squares technique) are satisfactorily described by the Gaussian function (10) up to about $3.6\,\sigma_{V/I}$, where $\sigma_{V/I}$ is the standard deviation of V/I. It means that the level of significance now does correspond to the Gaussian statistics (the Laplace function). The value $> 3.6\,\sigma_{V/I}$ is the deviation expected for one among $\sim$4000 pixels in the V/I spectrum in the case of the Gaussian statistics.

However, a small number of points have larger deviations seen, for instance, in the left part of Fig. 3. Weak cosmic ray traces, invisible in the intensity spectra but affecting the circular polarization spectra may be the source of such deviations. Therefore, we excluded from our analysis all the pixels showing residual deviations exceeding $3.6\,\sigma_{V/I}$. It changes the measured magnetic field by a magnitude, as a rule, not exceeding the statistical deviations of the measured mean longitudinal magnetic field $\langle B_z \rangle$; however, exceptions occur.

The last three columns of Table 1 illustrate the cumulative influence on $\langle B_z \rangle$ of the reduction of V/I and I spectra for the I continuum inclination (discussed in previous Section 6), and of the strongly deviating residuals (briefly discussed in this section). These reductions are applied to the V/I and I spectra pre-cleaned from (a) nonphotospheric spectral features (Section 4.3) and (b) the slopes of V/I continua (Section 5.4). Column 7, B_3, lists the LST–calculated $\langle B_z \rangle$ based on the spectra that have undergone the just–mentioned two first steps, (a) and (b) of cleaning. The last column of Table 1, B_4, contains $\langle B_z \rangle$ the values determined by the LST applied to the same spectra after their additional reductions described (c) in Section 6 and (d) above in the current Section 7.

We consider the values given in the last column of Table 1 as the final results of the LST measurements of the stellar mean longitudinal magnetic field strength $\langle B_z \rangle$ values.

Column 8, ΔB_3, in Table 1 presents the differences between the $\langle B_z \rangle$ values that appear as a result of the last two steps, (c) and (d) of the observed data reduction. As we see, these steps together can, in our sample, change the values of $\langle B_z \rangle$ up to $\pm(20-50)$ G, but in $\sim 70\,\%$ of spectra $|\Delta B_3| \leq 13$ G.

Similarly to the conclusions following from the previous corrections (a) and (b) we establish that the values of the corrections shown in column ΔB_3 in $\sim 30\,\%$ of spectra are comparable to or exceed the measurement accuracy, and therefore should be taken into account.

8 Discussion

We analyzed four factors that can make a bias in the resulting stellar mean longitudinal magnetic field $\langle B_z \rangle$ measured by the statistical method based on the least squares technique. This method, briefly described in Section 3 uses simultaneously all the numerous observed spectral lines in the intensity I spectrum, and the Zeeman features of the lines in the spectrum of circular polarization

degree $p_V = V/I$. The $\langle B_z \rangle$ bias are the most important ones for measuring mainly weak $\langle B_z \rangle \lesssim 200 - 300$ G).

Quantitative results are given for the set of our 13 FORS1 8.2 m VLT spectropolarimetric observations of the famous high massive black hole, an X–ray binary star Cyg X–1 = HDE 226868 with an O9.7 supergiant main component. The star's characteristics and observations are described in Section 4. A weak and variable $\langle B_z \rangle \sim 100$ G of the Cyg X–1 optical counterpart (the O–supergiant) was discovered by Karitskaya et al. (2009, 2010, 2011).

The tendencies of stellar magnetic field measurements show an increase of interest to distant high luminosity OB–stars. Many such stars (in contrast to the majority of the previously studied ones) show a large extinction and linear polarization (up to $p_{IS\ lin} \simeq 10\,\%$), mainly of interstellar or/and circumstellar origin. The HDE 226868 = Cyg X–1 optical counterpart belongs to this category ($p_{IS\ lin} \simeq 5\,\%$).

A significant part of the OB–binaries possess variable intrinsic linear polarization produced by the electron scattering of the binary components' radiation. Our sample object Cyg X–1 has a small ($\Delta p_{in\ lin} = \pm 0.1\,\%$), variable in accordance with the orbital phase, and with the intrinsic linear polarization. In the general case it is necessary to take into account a possible deformation of the Zeeman waves in the V/I spectrum by the cross–talk of spectral line features that can be present in the spectrum of linear polarization. Using the published data of Nagae et al. (2009) for the Cyg X–1 linear polarization spectrum, we show that the deformation most likely does not distort significantly the Zeeman waves and, consequently, the $\langle B_z \rangle$ measurement.

In addition to linear polarization, a part of hot luminous stars (including Cyg X–1) also have a tiny ($p_V < 0.05\,\%$) optical continual interstellar or/and intrinsic circular polarization. Thus, our sample object Cyg X–1 is a proper target for testing the influence of various obstacles to the weak stellar magnetic field measurements.

Obstacles similar to the above–mentioned are expected to be ever more frequent in the search for weak magnetic fields in distant hot luminous stars. For overcoming the obstacles successfully, it is necessary to adopt the widely used statistical method of $\langle B_z \rangle$ measurement to new conditions, based on the LST. The intensity I spectrum as well as the spectrum of the circular polarization degree $p_V = V/I$ are found to be polluted by interstellar features. Sharp interstellar lines, numerous diverse diffuse interstellar bands (DIBs), and the interstellar extinction distort the I spectrum. The extinction attenuates selectively the I–continuum and changes its slope.

The V/I spectrum is distorted by the interstellar features mainly via the cross–talk with the linear polarization: an unavoidable conversion of a small part of the linear polarization into the circular one due to the non-ideality of the retarding plate. In the optical range, the interstellar linear polarization has a purely continuum spectrum. The cross–talk converts it into a spurious V/I continuum $C_{V/I}$. Interstellar circular polarization can add to $C_{V/I}$. As it follows from Section 5, a sloped $C_{V/I}$ can strongly distort the $\langle B_z \rangle$ estimation, and should be removed. In our sample observations, the slope creates the $\langle B_z \rangle$ bias up to 100 G. It is greater than other biases considered in this paper. Moreover, it is probably the least obvious one. Therefore, we put the largest attention particularly to this kind of biases in the present paper.

The last kind of the $\langle B_z \rangle$ bias considered briefly in the paper is a result of the effect of deviating points. There are the points in the V/I spectra deviating from the V/I continuum by $(5-15)\,\sigma_{V/I}$. It is not a "useful signal" (Zeeman waves) because the deviations are one or two pixel–wide, which is less than one element of spectral resolution $\Delta\lambda \approx 3$ pixels, and the maximum of the "useful signal" does not exceed $(0.5-1)\,\sigma_{V/I}$. The value $\varepsilon_i > 3.6\,\sigma_{V/I}$ is the deviation expected for one of the ~ 4000 pixels in the V/I spectrum in the case of the Gaussian statistics (10), and (11) of the deviations ε_i. Therefore, we excluded all the pixels showing residual deviations ε_i exceeding $3.6\,\sigma_{V/I}$ from our analysis. One possible source of large deviations are the very weak cosmic ray traces, not visible in the I spectra. For a more accurate analysis we calculated the distribution of the residuals,

and found that the distribution agrees with the Gaussian function (10) up to $\varepsilon_i \approx 3.6\,\sigma_{V/I}$.

In the sample set of 13 VLT FORS1 spectropolarimetric observations of the O9.7 supergiant, the four considered corrections partially compensate each other. Thus, the total corrections of $\langle B_z \rangle$ do not exceed about 70 G only. But in other cases the corrections could be summarized. Indeed, if, e. g., the direction of the Cyg X–1 longitudinal magnetic field was opposite to the observed one, or/and the interstellar linear polarization had another orientation, the total correction could possibly reach the sum of the absolute values of corrections listed in Table 1 $|\Delta B_1| + |\Delta B_2| + |\Delta B_3|$, i. e., up to 150 – 200 G.

9 Conclusions

Four kinds of factors polluting the primarily processed spectropolarimetric observational data (the spectra of intensity I and the degree of circular polarization V/I) which can make a bias of the results of the mean longitudinal magnetic field $\langle B_z \rangle$ measurements by the least–squares–technique–based statistical method are considered in this paper. To exclude the biases and get the correct $\langle B_z \rangle$ it is necessary, before applying the LST to the "raw" (polluted) I and V/I spectra, to "clean" them, i. e., to remove the factors capable of distorting the result of the $\langle B_z \rangle$ measurement. Namely, it is necessary:

a) to exclude all the fragments of both I and I/V spectra containing the features formed outside the stellar photosphere (Section 4.3);

b) to remove the V/I spectrum slope (Section 5) and to be sure of the absence of distortion of the Zeeman features by the cross–talk from the linear polarization (Section 5.2), if present;

c) to normalize I to the pseudo–continuum including broad diffuse interstellar bands (DIBs) (Section 6);

d) to exclude from the analysis all the wavelength points λ_i (pixels) showing residual deviations exceeding $\simeq 3.5\,\sigma_{V/I}$ (Section 7).

Each reduction of the spectrum produces a new value of $\langle B_z \rangle$. The differences between the new and previously determined values are given in the columns of Table 1, titled ΔB_1, ΔB_2 and ΔB_3 for the sample of 13 FORS1 VLT spectropolarimetric observations of Cyg X–1 = HDE 226868. The first two corrections reach up to about ±100 G each (see Table 1). The sum of the last two corrections is found to be not greater than 50 G (see the ΔB_3 column). Although for Cyg X–1 the corrections partially cancel each other and the total correction of $\langle B_z \rangle$ does not exceed 70 G, the potential total correction can reach about 200 G.

Thus, the four steps of the observational data cleaning from the features that can distort the results of the $\langle B_z \rangle$ measurements by the LST statistical method we discuss here, should be kept in mind for any use of the above method, and be taken into account if the formal field measurement accuracy is $\sigma_{\langle B_Z \rangle} \lesssim 100$ G. It means that at least for stars with a significant interstellar extinction ($A_V \gtrsim 1^m$), and with $\langle B_z \rangle \lesssim 300$ G, the observed spectropolarimetric data should be subject to a multistep cleaning process described in this paper before using the data for magnetic field measurements applying the LST statistical method.

Acknowledgements. We are grateful to the ESO for granting the VLT observations in the service mode (programs 079.D–0549 and 381.D–0138). We thank S. Hubrig, M. I. Pogodin and M. Schöller for stimulating discussions, S. Hubrig and M. Schöller for the preliminary processing of the observational data and several test calculations made at an early stage of this research. This study was supported by the Russian Foundation for Basic Research (project nos. 09–02–00993 and 09–02–01136).

References

Bagnulo S., Landstreet J.D., Mason E., Andretta V., Silaj J., Wade G. A., 2006, A&A, 450, 777
Bagnulo S., Szeifert T., Wade G.A., Landstreet J. D., Mathys G., 2002, A&A, 389, 191
Gies D.R. Bolton C.T., Thomson J.R., Huang W., McSwain M. V., Riddle R. L., Wang Z., Wiita P. J., Wingert D. W., Csák B., Kiss L. L., 2003, ApJ, 583, 424
Hubrig S., Schöller M., Schnerr R.S., González J. F., Ignace R., Henrichs H. F., 2008, A&A, 490, 793
Hubrig S. Szeifert T., Schöller M., Mathys G., Kurtz D. W., 2004, A&A, 415, 685
Isobe T., Feigelson E. D., Akritas M. G., Babu G. J., 1990, ApJ364, 104
Karitskaya E.A., 2007, in: Mashonkina L., Sachkov M. (eds), Proc. Int. Conf., "Spectroscopical Methods in Modern Astrophysics", Yanus–K, Moscow, 67 [in Russian]
Karitskaya E. A., Bochkarev N. G., Bondar' A. V., Galazutdinov G. A., Lee B.–C., Musaev F. A., Sapar A. A., Shimanskii V. V., 2008, Astronomy Reports, 52, 362
Karitskaya E. A., Bochkarev N. G., Hubrig S., Gnedin Yu. N., Pogodin M. A., Yudin R. V., Agafonov M. I., Sharova O. I., 2009, astro–ph 0908.2719
Karitskaya E. A., Bochkarev N. G., Hubrig S., Gnedin Yu. N., Pogodin M. A., Yudin R. V., Agafonov M. I., Sharova O. I., 2010, IBVS, 5950, 1
Karitskaya E. A., Bochkarev N. G., Hubrig S., Gnedin Yu. N., Pogodin M. A., Yudin R. V., Agafonov M. I., Sharova O. I., 2011, in this volume
Landstreet J. D., 1982, ApJ, 258, 639
Michalsky J. J., Swedlung J. B., 1977, ApJ, 212, 221
Nagae O., Kawabata K. S., Fukazawa Y., Okazaki A., Isogai M., 2009, AJ, 137, 3509